Spatial representation of temporal information through spike-timing-dependent plasticity

Thomas Nowotny* and Misha I. Rabinovich†
Institute for Nonlinear Science, University of California, San Diego, 9500 Gilman Drive, La Jolla, California 92093-0402, USA

Henry D. I. Abarbanel‡
Institute for Nonlinear Science, Department of Physics, University of California, San Diego, La Jolla, California 92093-0402, USA and Marine Physical Laboratory (Scripps Institution of Oceanography), University of California, San Diego, La Jolla, California 92093-0402, USA

(Received 3 September 2002; revised manuscript received 24 February 2003; published 18 July 2003)

We suggest a mechanism based on spike-timing-dependent plasticity (STDP) of synapses to store, retrieve and predict temporal sequences. The mechanism is demonstrated in a model system of simplified integrate-and-fire type neurons densely connected by STDP synapses. All synapses are modified according to the so-called normal STDP rule observed in various real biological synapses. After conditioning through repeated input of a limited number of temporal sequences, the system is able to complete the temporal sequence upon receiving the input of a fraction of them. This is an example of effective unsupervised learning in a biologically realistic system. We investigate the dependence of learning success on entrainment time, system size, and presence of noise. Possible applications include learning of motor sequences, recognition and prediction of temporal sensory information in the visual as well as the auditory system, and late processing in the olfactory system of insects.

DOI: 10.1103/PhysRevE.68.011908 PACS number(s): 87.19.La, 87.10.+e, 87.19.−j

I. INTRODUCTION

Animals are challenged in various ways to learn, produce, reproduce and predict temporal patterns. For example, numerous motor programs are necessary to interact efficiently with the environment. One specific manifestation is the vocal motor system of song birds. It has been shown that the temporal sequence of syllables in a bird's song corresponds to temporal sequences of bursts in the neurons of the forebrain control system [1–3]. These are learned and stored by the adolescent bird.

Temporal codes seem to be used for a variety of other tasks as well. Temporal coding in the retina [4] is an example, as is information transport in the olfactory system of the locust. In the latter it has been shown that the purely identity coded information of the receptor neurons is transformed into an identity-temporal code inside the antennal lobe [5–7].

Whereas there is a long history of research on sequence learning and recognition in the framework of abstract neural networks (cf. the relevant chapters in Refs. [8,9] and references therein), it is an open question how the learning and memory of time sequences is accomplished in real biological neural systems. Three main principles for representing time in neural systems are frequently discussed:

(1) The first makes use of delays and filters. There are various ways of processing temporal information in the dendritic tree [10–13] or through axonal delays [14–20]. Other examples are multilayer neural networks in which the delay of the synaptic connections between layers allows to represent or decode temporal information and propagating waves, as known from the thalamo-cortical system [21,22].

(2) The second principle rests on feedback. Through delayed feedback temporal information can be processed on the level of individual neurons as well as on the level of larger structures. A prominent example for this are recurrent multilayer neural networks which play a role in sequence memory in the hippocampus [23,24].

(3) The third principle is to transform the temporal information into spatial information. This can occur through the dynamics of a network with asymmetric lateral inhibition [25].

In this paper we demonstrate an alternative mechanism that maps the temporal information to the strength of synapses in a network through spike-timing-dependent plasticity (STDP). Similar mechanisms have been suggested for predictive activity and direction selectivity in the visual system [26] and learning in the hippocampus [23,24,27] as well as prediction in hippocampal place fields and route learning in rats [28–30]. In contrast to these earlier works, we focus on questions of learning of several distinct input sequences in one system and a sparse coding scheme. This learning capability is necessary in order to process the identity-temporal code believed to be generated by winnerless competition in sensory systems [7,31].

Synaptic plasticity in the connections among neurons allows networks to alter the details of their interaction and develop memories of previous input signals. The details of the methods by which biological neurons express plasticity at synapses are not fully understood at the biophysical level, but many aspects of the phenomena which occur when presynaptic and postsynaptic neurons are jointly activated are now becoming clear. First of all, it seems well established that activity at both the presynaptic and the postsyn-

*Electronic address: tnowotny@ucsd.edu; URL:http://inls.ucsd.edu/~nowotny
†Electronic address: mrabinovich@ucsd.edu
‡Electronic address: hdia@jacobi.ucsd.edu

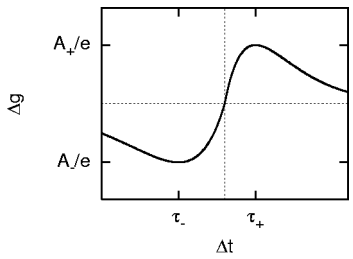

FIG. 1. Spike-timing-dependent plasticity learning rule. $\Delta g = A_+ \Delta t/\tau_+ e^{-\Delta t/\tau_+}$ for $\Delta t > 0$ and $\Delta g = A_- \Delta t/\tau_- e^{\Delta t/\tau_-}$ for $\Delta t < 0$, A_+, $A_- > 0$. This form of the learning rule was directly inferred from experimental data [37].

aptic parts of a neural junction is required for the synaptic strength to change. Arrival of a presynaptic action potential will induce, through normal neurotransmitter release and reception by postsynaptic receptors, a postsynaptic electrical action which generally leads to no change in the coupling strength at that synapse. Depolarization of the postsynaptic cell by various means *coupled with* arrival of a presynaptic action potential can lead to changes in synaptic strength in a variety of experimental protocols. It is quite important that changes in the synaptic strength, which we denote in terms of a conductivity change Δg can be either positive, called potentiation, or negative, called depression. When the expression of Δg is long lasting, several hours or even much longer after induction, increases in g are called long term potentiation or LTP, and decreases in g are called long term depression or LTD. Good reviews of the current situation are found in Refs. [32–34].

LTP and LTD can be induced by (1) depolarizing the postsynaptic cell to a fixed membrane voltage and presenting presynaptic spiking activity at various frequencies, by (2) inducing slow (LTD) or rapid (LTP) release of Ca^{2+} [35], or by (3) activating the presynaptic terminal a few tens of milliseconds before activating the postsynaptic cell, leading to LTP, or presenting the activation in the other order, leading to LTD [36,37].

In this paper we study numerically a network composed of integrate-and-fire neurons which are densely coupled with synaptic interactions whose maximal conductances are permitted to change, in accordance with the observations on closely spaced spike arrival times, to the presynaptic and postsynaptic junctions of the synapse.

The response of a learning synapse to the arrival of a presynaptic spike at $t_{\rm pre}$ and a postsynaptic spike at $t_{\rm post}$ is a function only of $\Delta t = t_{\rm post} - t_{\rm pre}$ and for $\Delta t > 0$, $\Delta g(\Delta t)$ is positive (LTP), and for $\Delta t < 0$, $\Delta g(\Delta t)$ is negative (LTD).

$$\Delta g(\Delta t) = A_+ \frac{\Delta t}{\tau_+} e^{-\Delta t/\tau_+} \quad \text{for} \quad \Delta t > 0,$$

$$\Delta g(\Delta t) = A_- \frac{\Delta t}{\tau_-} e^{\Delta t/\tau_-} \quad \text{for} \quad \Delta t < 0, \tag{1}$$

where A_+, A_-, τ_+, and τ_- are positive constants (see Fig. 1). Synaptic plasticity of this type is often referred to as spike-timing-dependent plasticity. For many mammalian *in vitro* or cultured preparations, the characteristic LTD time τ_- is about two or three times longer than the characteristic LTP time τ_+.

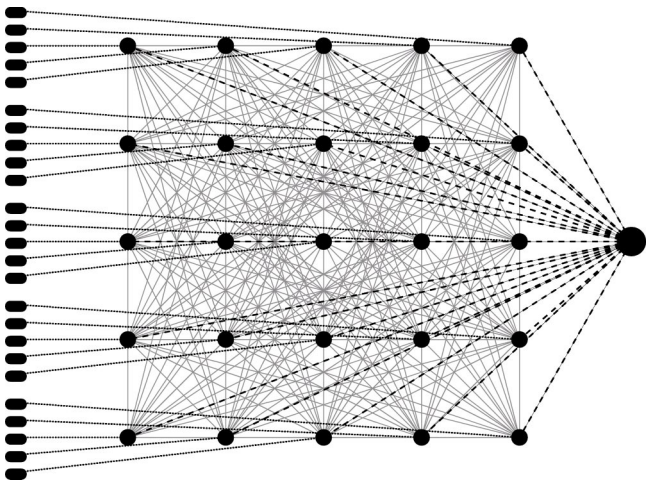

FIG. 2. Morphology of the model system. The ovals are artificial input neurons producing rectangular spikes of 3 ms duration at specified times. Each is connected by a nonplastic excitatory synapse to one of the neurons in the main "cortex" (dotted lines). The full circles depict the integrate-and-fire neurons of the main cortex. They are connected all-to-all by spike-timing-dependent-plasticity synapses shown as solid gray lines. The big full circle on the right depicts a neuron with slow Calcium dynamics which inhibits all neurons in the cortex through the nonplastic synapses shown as dashed lines.

Here we inquire how a network composed of familiar integrate-and-fire neurons can develop preferred spatial patterns of connectivity when interacting through synapses that update their strength according to the STDP learning rule just given. This rule is a simplification, which applies to our setting of spiking neurons, of more general models [38–44] that indicate how $\Delta g(\Delta t)$ behaves under stimulus of arbitrary presynaptic and postsynaptic wave forms.

The transformation of temporal information into synapse strength through STDP maps a temporal sequence of excitations of neurons to a chain of stronger or weaker synapses among these neurons. If the synapses are excitatory, a strengthened chain of synapses facilitates subsequent excitations of the same temporal pattern up to a point where activation of a few neurons from the temporal sequence allows the system to complete the remaining sequence. The temporal sequence thus has been learned by the system. We demonstrate this type of sequence learning in a computer simulation of a system with integrate-and-fire neurons and Rall-type synapses, and investigate the reliability of learning, the storage capacity in terms of the number of stored sequences, the scaling of both with system size and sequence length, and the robustness against different types of noise.

II. MODEL SYSTEM

A. Components and connections

To explore the learning principle, we simulated a network with the topology shown in Fig. 2. In this network, n

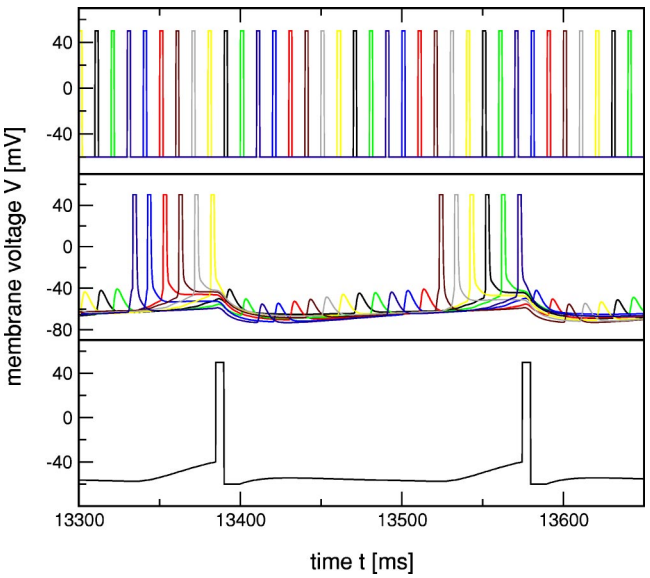

FIG. 3. Typical piece of a training session. The rectangular spikes in the upper panel are the input signal spaced by 10 ms in this example. The traces in the middle panel are the integrate-and-fire memory neurons. The slow spike train in the bottom panel belongs to the globally inhibitory neuron. Note the instantaneous onset of the spikes in the integrate-and-fire neurons and how the inhibitory neuron segments the input into pieces of six spikes each.

integrate-and-fire neurons are connected all-to-all while each neuron also receives input from one ''input neuron'' (filled ovals in Fig. 2).

The input neurons generate rectangular spikes of 3 ms duration at times determined by externally chosen input sequences. Each of these spikes is sufficient to trigger exactly one spike in the receiving neuron (see Fig. 3). The input sequences are chosen such that only one input neuron spikes at any given time and the time between input spikes was fixed in the normal test setup. In Sec. IV these input neurons are replaced by Poisson neurons with random spike times.

The membrane voltage of the integrate-and-fire neurons used in this study for subthreshold activity is given by

$$C\frac{dV}{dt} = -g_{\mathrm{leak}}[V(t) - V_{\mathrm{leak}}] + I_{\mathrm{synapse}}(t), \tag{2}$$

where $C = 0.2$ nF, $g_{\mathrm{leak}} = 0.3\ \mu$S, and $V_{\mathrm{leak}} = -60$ mV. Whenever membrane potential $V(t)$ reaches $V_{\mathrm{th}} = -40$ mV, it is set to firing voltage $V_{\mathrm{max}} = 50$ mV, kept at that voltage for $t_{\mathrm{fire}} = 2$ ms and then released into the normal integration state. The neuron is subsequently refractory for $t_{\mathrm{refract}} = 40$ ms before another firing event is allowed. During the refractory period the neurons integrate normally but the transition of the firing threshold has no effect. In the implementation of integrate-and-fire neurons used in this work, no crossing of the firing threshold from below is necessary to elicit a spike in a super-threshold neuron after the refractory period. See Fig. 3, middle panel, for typical spike forms.

A neuron connected to all neurons in the network (large filled circle in Fig. 2) provides global inhibition whenever the activity in the network exceeds a certain threshold. The inhibitory neuron is an integrate-and-fire neuron governed by Eq. (2) with $C = 1.0$ nF, $g_{\mathrm{leak}} = 0.01\ \mu$S, $V_{\mathrm{leak}} = -60$ mV, $V_{\mathrm{th}} = -40$ mV, $V_{\mathrm{max}} = 50$, and $t_{\mathrm{fire}} = 5$ ms. In contrast to the memory neurons this neuron is reset to its resting potential V_{leak} after each firing. Then the membrane potential is fixed to V_{leak} for $t_{\mathrm{refract}} = 10$ ms until normal integration resumes. The inhibitory neuron was implemented as a resetting integrate-and-fire neuron because it has a very weak leak current allowing integration over long time windows. This weak leak current would cause very unnatural broad spikes in a nonresetting neuron. A typical voltage trace is shown in the lowest panel of Fig. 3.

Our model of the synapses comes from Rall [45,46] and now is a standard model for simplified synaptic dynamics [47]. In particular, we use

$$I_{\mathrm{synapse}} = -g_{\mathrm{syn}}\, g(t)[V_{\mathrm{post}}(t) - V_{\mathrm{syn}}], \tag{3}$$

where $g(t)$ satisfies

$$\frac{df(t)}{dt} = \frac{1}{\tau_{\mathrm{syn}}}[\Theta(V_{\mathrm{pre}}(t) - V_{\mathrm{th}}) - f(t)],$$

$$\frac{dg(t)}{dt} = \frac{1}{\tau_{\mathrm{syn}}}[f(t) - g(t)], \tag{4}$$

and $V_{\mathrm{syn}} = 0$ mV, $V_{\mathrm{th}} = -20$ mV, $\tau_{\mathrm{syn}} = 15$ ms, $V_{\mathrm{pre}}(t)$ and $V_{\mathrm{post}}(t)$ are the pre and postsynaptic membrane potentials, and g_{syn} is the strength of the synapse. $\Theta(u) = 0, u \leqslant 0$ and $\Theta(u) = 1, u > 0$ is the usual Heaviside function. Typical excitatory postsynaptic potentials (EPSPs) generated by these synapses can be seen in the middle panel of Fig. 3.

The synaptic strength of the internal synapses is adjusted according to the synaptic plasticity rule shown in in Fig. 1 whenever a spike in their presynaptic and postsynaptic neuron occurs. In itself, this rule may lead to ''run-away'' behavior of the synaptic strengths. While this may be avoided in the dynamical model of synaptic plasticity [44], we need to address this within the simpler model used here. We do so by two approaches:

(1) We add a long term, slow decay to the synaptic plasticity which would, all other factors being absent, bring it back to a nominal allowed level a long time after alteration by our rule. This we implement with

$$\frac{dg_{\mathrm{raw}}}{dt} = -\frac{1}{\tau_g}[g_{\mathrm{raw}}(t) - g_{0,\mathrm{raw}}], \tag{5}$$

where $g_{0,\mathrm{raw}}$ is the initial value of the unmodified synapse strength. So, after potentiation or depression according to the synaptic plasticity rule, the synaptic strength is allowed to slowly decay back to its original value. The time scale of this exponential decay is set by $\tau_g = 200$ s.

(2) g_{raw} is an intermediate variable which is then translated into synaptic strength g_{syn} via a sigmoid saturation rule:

$$g_{\mathrm{syn}} = g_{\mathrm{max}}\frac{1}{2}[\tanh(g_{\mathrm{slope}}(g_{\mathrm{raw}} - g_{1/2})) + 1], \tag{6}$$

where $g_{\max}$ is the largest allowed value for the synaptic conductivity, and $g_{1/2}$ sets the threshold where saturation to this value is implemented. All data shown in this work was obtained with $g_{\max}=2.8\ \mu$S, $g_{1/2}=1/2\,g_{\max}$, and $g_{\text{slope}}=1/g_{1/2}$. In addition, the globally inhibitory neuron tends to curb the tendency of the network to saturate its synaptic strengths.

These features of our model reflect our lack of knowledge of the biophysical factors setting the synaptic strength, in the first place, and our equivalent lack of knowledge of how these factors bound the eventual rise or fall of synaptic strength. Our assumption in using these rules is that the actual mechanisms, while surely more complicated in detail, will provide the same effective bounding feature.

The complete system is realized in C++ using an order 6(5) variable time step Runge-Kutta algorithm [48]. The error goal per time step was 10^{-7} in all simulations. A run of 100 simulated seconds of a system with 50 neurons takes about three hours on an Athlon 1.4 GHz processor.

This model system mimics the situation of a highly connected piece of cortex receiving input from the neural periphery. Our input can be interpreted in two ways. It might be a single strong EPSP received from an upstream neuron, which is strong enough to trigger a spike. It could also be interpreted as the coincidence of several weaker EPSPs received from various presynaptic neurons being sufficient to cause a spike.

B. Operations and activity

To test the ability of this network to store (learn) and retrieve (remember) temporal-identity patterns, it was trained with sets of randomly chosen sequences of inputs. These sequences were chosen without repetition of neurons within the sequence. Note that this implies a minimal time of the order of the length of the sequence between spikes in each neuron. For this reason, the choice of resetting or nonresetting neurons is not important as the integration times of the neurons are small compared to the total length of the sequences and the time scale of the global inhibition. Our choice of nonresetting integrate-and-fire neurons was mainly guided by the more natural spike form of the nonresetting variety.

The sequences were presented continuously, with the first neuron of the sequence following the last with the same time delay as the neurons within the sequence. The global inhibition of the system partitions this continuous input of spikes into pieces of about 6–8 spikes at a time. Between these input windows the whole system is inhibited and thus reset. This mechanism can be seen in the example training session shown in Fig. 3. Note that the details of the global inhibition mechanism do not matter as long as the system is efficiently reset after an appropriate amount of activity.

Learning rate A_+ and time scale of forgetting τ_g in the synaptic plasticity learning rule were chosen such that learning reaches a steady state after a learning time of about $1600\Delta t$, where Δt is the fixed interspike interval between input activations. For an example of the learning protocol see Fig. 3. In all studies described below, Δt was chosen as $\Delta t = 10$ ms, 15 ms, or 20 ms. The learning rule has to accommodate all these input speeds and possibly values in between. In particular, we chose here $A_+=0.3\ \mu$S, $A_-=2/3A_+$, $\tau_+=16$ ms, $\tau_-=3/2\tau_+$, and $\tau_g=200$ s.

After the training phase the network was presented with pieces of the training patterns. We presented all possible ordered pieces of one to four input spikes and recorded the number and identity of spiking neurons in the network in response to this input. Perfect learning of the patterns would correspond to obtaining a spike from each of the network neurons in a given pattern when presenting a piece of two or three inputs from that pattern to the input neurons. Furthermore, all other network neurons should remain inactive if the pattern is reproduced exactly.

As a result of incomplete or ineffective learning two types of errors can occur. (1) Neurons that should be excited within the given pattern do not spike or (2) neurons that are not supposed to spike do so. Due to overlap of input patterns, the learning efficiency is a function of the number of learned patterns as well as the size of the network. Therefore, estimating the expected amount of overlaps in the randomly chosen input sequences provides information about the optimally achievable system performance.

The probability distribution for number Y_{ijrkn} of *ordered* j-tuples occurring in at least i out of r patterns with k neurons each for a system with a total number of n neurons can be calculated in the following way. First consider a given ordered j-tuple and a given pattern with k neurons. The sequence is presented continuously and, therefore, needs to be interpreted as cyclically closed. Thus, there are k possibilities to position the j tuple in the sequence (starting at neuron 1 to starting at neuron k) and $(n-j)!/[n-j-(k-j)]!$ possibilities to choose the remaining neurons in the sequence. The total number of sequences of length k is $n!/(n-k)!$. Therefore, probability p_j to have a given ordered j-tuple in a given pattern with k active neurons is given by

$$p_j=k\frac{(n-j)!}{(n-k)!}\Big/\frac{n!}{(n-k)!}=k\frac{(n-j)!}{n!}. \tag{7}$$

If r sequences of length k are chosen independently, the probability to have any given ordered j-tuple of neurons in i or more of the r sequences is given by the binomial distribution with parameters r and p_j,

$$p_j^i=\sum_{s=i}^{r}\binom{r}{s}(p_j)^s(1-p_j)^{r-s}. \tag{8}$$

In good approximation one can assume the events of one given j-tuple being in i or more sequences and another j-tuple being in i or more sequences to be independent. In this approximation, the probability distribution for Y_{ijrkn} is again a binomial distribution with parameters $n!/(n-j)!$ and p_j^i,

$$P(Y_{ijrkn}=l)\approx\binom{\dfrac{n!}{(n-j)!}}{l}(p_j^i)^l(1-p_j^i)^{[n!/(n-j)!]-l}. \tag{9}$$

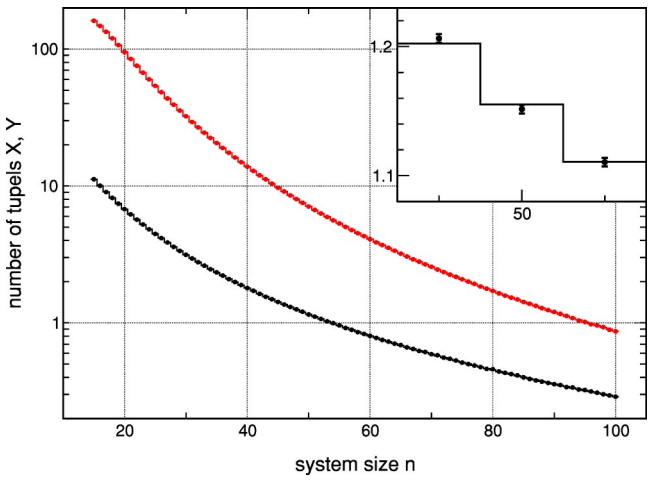

FIG. 4. Comparison of the expectation values for $Y_{2,2,10,8,n}$ (lower line) and $X_{2,3,10,8,n}$ (upper line) obtained from Eqs. (9) and (12) to the normalized number of occurrences of unordered three-tuples (gray dots) and ordered two-tuples (black dots) in more than two sequences in 100 000 randomly generated sets of ten sequences of length 8. The inlay shows a closeup of the data on ordered tuples in the region with system size around 50 neurons, which is the size used in most numerical simulations.

Figure 4 shows a comparison of the expectation value for $\mathbf{E}Y_{2,2,10,8,n}$ obtained from this approximate distribution compared to the relative number of occurrences in 100 000 randomly generated sets of ten sequences of length 8. The lack of a significant discrepancy demonstrates the precision of the estimate.

The probability distribution for number X_{ijrkn} of *unordered* j-tuples occurring in at least i out of r patterns with k neurons each for a system with a total number of n neurons can be calculated pretty much in the same way. Now, probability $\hat{p}_j$ to have a given unordered j-tuple in a given pattern with k active neurons is

$$\hat{p}_j = \binom{n-j}{k-j} \Big/ \binom{n}{k}. \tag{10}$$

Then, probability $\hat{p}_j^i$ to have any given unordered j-tuple of neurons in i or more of r independently chosen patterns is the binomial distribution with parameters r and $\hat{p}_j$,

$$\hat{p}_j^i = \sum_{s=i}^{r} \binom{r}{s} (\hat{p}_j)^s (1-\hat{p}_j)^{r-s}. \tag{11}$$

Again taking the approximation of assuming independence for the occurrence of distinct tuples, this leads once more to a binomial distribution, now with parameters $\binom{n}{j}$ and $\hat{p}_j^i$,

$$P(X_{ijrkn}=l) \approx \binom{\binom{n}{j}}{l} (\hat{p}_j^i)^l (1-\hat{p}_j^i)^{\binom{n}{j}-l}. \tag{12}$$

The comparison of expectation values $\mathbf{E}X_{2,3,10,8,n}$ with numerically observed relative numbers of occurrence in Fig. 4 shows again a perfect match.

The model parameters were chosen such that two to three spiking predecessors of a given neuron in a trained sequence are sufficient to excite that neuron. The learning performance is therefore poor as long as there is a significant amount of ordered two-tuple overlaps in the patterns. Rule of thumb $\mathbf{E}Y_{22rkn} < 0.5$ for the expectation value of Y_{ijrkn} provides an estimate for number r of pattern of length k that can be successfully stored in a system of n neurons. Another estimate for the number of learnable sequences is provided by rule of thumb $\mathbf{E}X_{23rkn} < 0.5$, i.e., the overlaps in input sequences should have negligible impact on the learning if there is no significant amount of *unordered* three-tuples occurring in more than one pattern.

Typically, capacity estimates are given in the limit of system size n tending to infinity. As shown in the Appendix, the leading term of the Taylor expansion of p_j^i with respect to p_j around $p_j = 0$ is

$$p_j^i = \binom{r}{i} (p_j)^i + O((p_j)^{i+1}) \tag{13}$$

such that asymptotic equation

$$\lim_{n\to\infty} \mathbf{E}Y_{ijrkn} \overset{!}{=} \epsilon \tag{14}$$

leads to

$$\lim_{n\to\infty} \frac{n!}{(n-j)!} \binom{r}{i} \left(k \frac{(n-j)!}{n!} \right)^i = \epsilon \tag{15}$$

$$\Leftrightarrow \lim_{n\to\infty} \frac{r^i}{i!} k^i n^{-j(i-1)} = \epsilon \tag{16}$$

such that capacity $r(n,k,\epsilon)$ is asymptotically

$$r(n,k,\epsilon) = \frac{1}{k} (i!\,\epsilon)^{1/i} n^{j(i-1)/i}. \tag{17}$$

In the same way,

$$\lim_{n\to\infty} \mathbf{E}X_{ijrkn} \overset{!}{=} \epsilon \tag{18}$$

leads to

$$\hat{r}(n,k,\epsilon) = \frac{(k-j)!}{k!} (i!\,j!\,\epsilon)^{1/i} n^{j(i-1)/i}. \tag{19}$$

The dashed lines in Fig. 5 are some examples for the first rule of thumb $\mathbf{E}Y_{22rkn} = \frac{1}{2}$ and the thin solid lines are the corresponding values of $r(n,k,\frac{1}{2})$. The estimates based on rule $\mathbf{E}X_{23rkn} = \frac{1}{2}$ are shown as dash-dotted lines in Fig. 5 and the corresponding values of the asymptotically correct $\hat{r}(n,k,\frac{1}{2})$ are again shown as thin solid lines. The correspon-

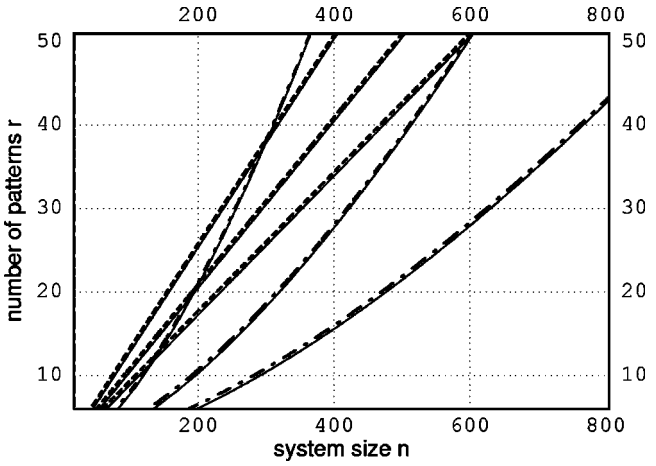

FIG. 5. Estimate for the maximum storage capacity of the system. The dashed lines divide the plane into two regions with $\mathbf{E}Y_{2,2,r,k,50} > 0.5$ (above) and $\mathbf{E}Y_{2,2,r,k,50} < 0.5$ (below) for $k=8$ (topmost line), 10 (middle line), and 12 (lowest line), respectively. The thin solid lines are the corresponding estimates for the asymptotically correct values $r(50,k,\frac{1}{2})$. The dash-dotted lines analogously mark the boundaries between regions with $\mathbf{E}X_{2,3,r,k,50} > 0.5$ (above) and $\mathbf{E}X_{2,3,r,k,50} < 0.5$ (below). Again the thin lines are the asymptotically correct estimates $\hat{r}(50,k,\frac{1}{2})$

dence between the exact evaluation of the capacity estimators and the asymptotically correct capacity functions $r(n,k,\epsilon)$ and $\hat{r}(n,k,\epsilon)$ is noteworthy. Relative capacities $r'(k) := kr(n,k,\epsilon)/n^{j(i-1)/i} = (i!\,\epsilon)^{1/i}$ and $\hat{r}'(k) := k\hat{r}(n,k,\epsilon)/n^{j(i-1)/i} = [(k-j)!/(k-1)!](i!\,j!\,\epsilon)^{1/i}$ behave quite differently. Whereas the former is constant with respect to k the latter is falling in k. So, depending on whether a system is more sensitive to ordered tuple overlaps or to unordered tuple overlaps, the relative capacity is constant or falling in k. In particular, for systems sensitive to unordered tuple overlaps, it will be beneficial to store many short sequences instead of a few long ones.

III. RESULTS

The synaptic plasticity allows one to store time sequences of excitation of neurons into patterns of strengthened synapses as intended. A simple example is shown in Fig. 6 for one input pattern. For randomly chosen input sequences, the patterns are structured in the same way but are not so easy to detect with the human eye. During training the synapses between consecutively active neurons are strengthened if pointing in the direction of the activation order or weakened if connecting the neurons in the wrong direction. An example of the development of the average synaptic strength of synapses between neurons of one out of five trained sequences is shown in Fig. 7. Note that the time course and final strength of the synapses depends on the speed with which the sequences are entrained due to the nonconstant learning curve (1).

The ability to store more than one pattern was tested in various setups. We mainly varied choice, number, and length of input sequences and the speed of entrainment.

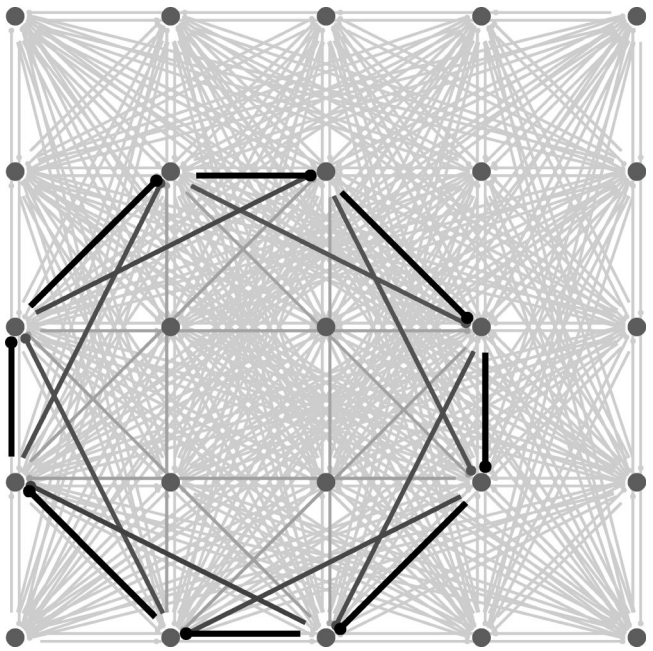

FIG. 6. Simple example of a learned identity-temporal pattern. The neurons at the corners of the octagon have been repeatedly excited in clockwise order. The width and grayscale of the connections encodes the strength of the corresponding synapse and the small circle at the end shows its direction. As one can clearly see, the temporal pattern is transformed into an ordered spatial pattern by synaptic plasticity.

A typical example for a network of 50 neurons trained with five sequences of length 8 is shown in Figs. 8 and 9. There are several important features to point out. First of all, the recall never comprises all eight neurons of the trained sequence but only up to seven active neurons. This is, however, not a universal feature but rather a characteristic of the global inhibition circuit shutting down the system after ca. 7 spike occurrences (see Fig. 8). Furthermore, note that the recall of the sequences speeds up toward the end of the sequence. This is partly due to the fact that the integrate-and-fire neurons used here do not have a finite rise time for their spikes, which allows them to instantaneously affect their postsynaptic neurons.

In a network with more realistic neurons one would expect that there is a lower limit on the speed with which sequences can be recalled in the system. Preliminary studies with realistic Hodgkin-Huxley-type neurons show this effect [49]. It has clear advantages for maintaining the correct order of recall in the system. The microscopic internal dynamics of the neurons thus seems to be non-negligible for the macroscopic performance of the system. This will be discussed in more detail in forthcoming work.

The quality of recall of sequences depends very much on the sequence and the piece presented as a cue. This is, however, also no surprise because sequence overlaps occur at certain neurons in the sequence and if these are used as a cue, the performance is worse than when other neurons are used. In Fig. 9 one can see how some sequences are reproduced very well and are error-free while others lead to activation of quite a few incorrect neurons.

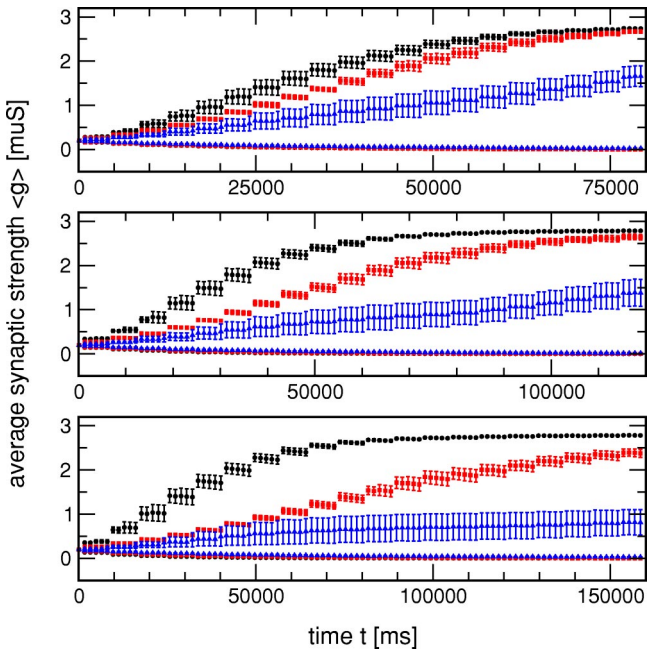

FIG. 7. Development of synaptic strength during training. The network of 50 neurons was trained with five sequences of length 8 in sequential order. The topmost panel shows the data for sequences entrained with interspike interval $\Delta t = 10$ ms, the middle with $\Delta t = 15$ ms, and the lowest with $\Delta t = 20$ ms. Each sequence was presented for $80\Delta t$ at a time. The data shown are average synaptic strengths of synapses between the neurons of one of the trained sequences. The topmost points are the average strengths of all synapses between the neurons and their direct successors in the sequence, the middle are the corresponding strengths of synapses between neurons who are next nearest neighbors in the sequence under consideration, and the lower points correspond to strengths of synapses between neurons with distance 3 in the sequence. The lowest data points are the strengths between the neurons of the sequence as described above but *against* the order of activation in the trained sequence. The sharp rises in synaptic strength correspond to training of the particular sequence shown here and the falling flanks correspond to the decay while other patterns are trained.

To test for the capacity of the system systematically, we trained a network of 50 neurons with two up to ten sequences of length 8. For each number of sequences five independent sets of randomly chosen sequences were tested. Figure 10 shows the average response of the trained systems to pieces of two inputs taken from the learned sequences. The averages are over all possible subsequences and all five input sequence sets for each data point. This experiment was done with three different input speeds, i.e., the input was presented with fixed interspike intervals of length $\Delta t = 10$ ms, 15 ms, and 20 ms. As one can see in Fig. 10 the performance dramatically decreases for the slowest entrainment speed. This is due to the fact that the fixed width of the learning window in Eq. (1) leads to weaker synapses for all the synapses in this case as spikes are separated further in time (see last row of Fig. 7). The minimum and maximum possible speed of the entrainment are thus directly determined by the learning window. If one chooses a larger learning window the slower

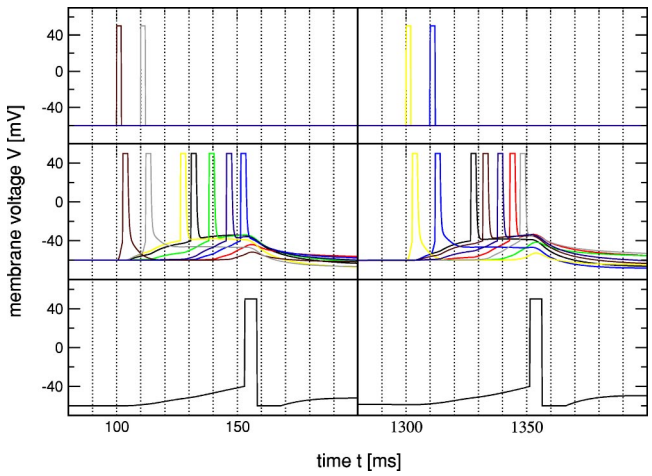

FIG. 8. Typical recall episodes. The system of 50 neurons was trained with two (left panel) or five (right panel) sequences for $1600\Delta t$ per sequence, where $\Delta t = 10$ ms. It then receives a cue of two spikes from one of the trained sequences and autonomously completes the sequence until stopped by the globally inhibitory neuron. Note that although the recall of the identity and order of the neurons is perfect in both cases, the exact timing is lost. In general, one sees a tendency of speedup to the end of the recalled sequence. This can have the effect of destroying the correct order of recall in the later sequence if the global inhibition is not present.

sequences could be entrained as well. However, this would also lead to decreased performance for faster sequences.

To test for the dependence of learning success on the length of presented sequences we entrained a 50 neuron system with sets of five sequences of length 6 to 9. Figure 11 shows the performance of the system. On first sight it is surprising that the system performs worse for shorter se-

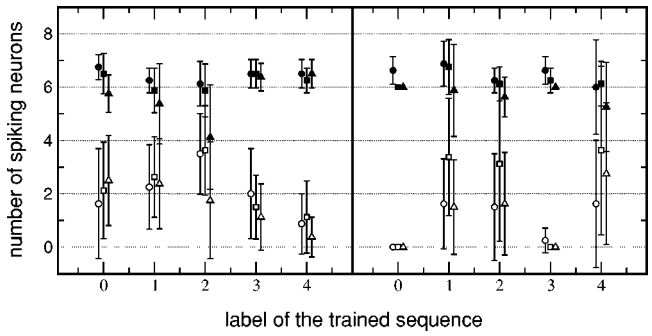

FIG. 9. Examples of learning in a 50 neuron network after $1600\Delta t$ sequential training with five input sequences of length 8. The left and the right panels show results for two independently chosen sets of five input sequences labeled with numbers 0 to 4 in each set. The filled symbols show the average number of spiking neurons within a tested sequence and the open symbols show erroneously spiking neurons. The test cue were fractions of length 2 from the trained sequences. The circles were obtained with a training speed of $\Delta t = 10$ ms, the squares with $\Delta t = 15$ ms, and the triangles with $\Delta t = 20$ ms. Note that the results depend on the structure of the input set. Whereas in the left case all sequences have some overlap, in the right case sequence 0 and sequence 3 are pretty much disjoint from the others.

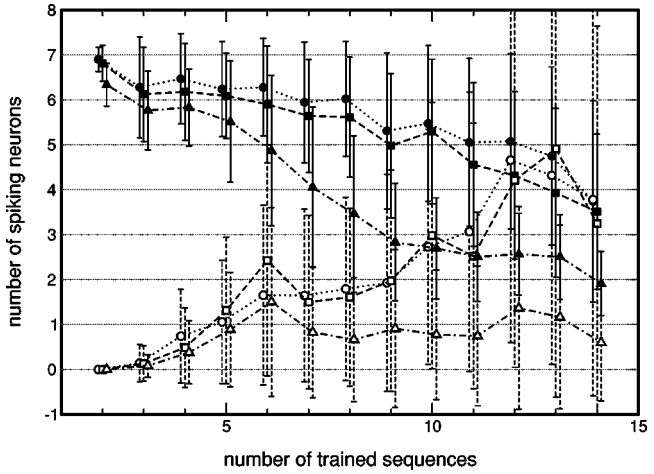

FIG. 10. Scaling of storage quality with the number of input sequences. A system with 50 neurons was trained with a varying number of input sequences of length 8. The figure shows the response after a total of $1600\Delta t$ training for each input sequence. The filled symbols show the average number of responding neurons within a tested sequence and the open symbols show the number of incorrectly responding neurons. The test cues were pieces of two inputs from the trained sequences. The circles were obtained with sequences trained with interspike intervals $\Delta t = 10$ ms, the squares with $\Delta t = 15$ ms, and the triangles with $\Delta t = 20$ ms. All data points are averages of trials with five independently chosen sets of input sequences.

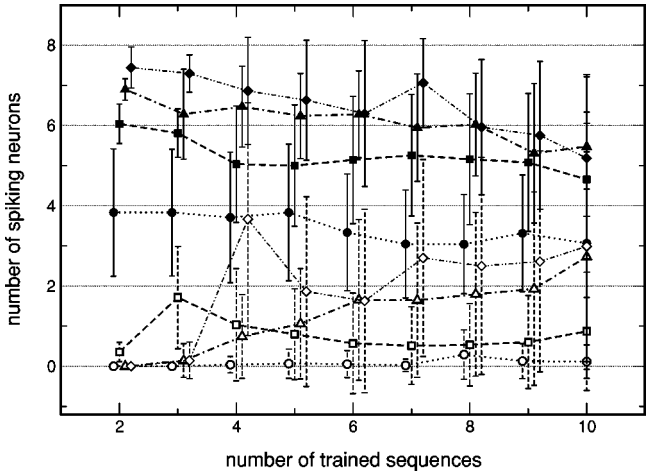

FIG. 11. Scaling of storage quality with the length of input sequences. A system with 50 neurons was trained with sets of five input sequences of different lengths. The figure shows the response after a total of 16 s training for each input sequence. The filled symbols show the average number of responding neurons within a tested sequence and the open symbols the number of incorrectly responding neurons. The test cues were pieces of two inputs from the trained sequences. The circles were obtained with sequences of length 6, the squares with length 7, the triangles with length 8, and the diamonds with length 9. All data points are averages of trials with five independently chosen sets of input sequences.

quences. Naively, one would expect a better performance because overlaps are less likely. Indeed, one can really see that the number of erroneous spikes is smaller. On the other hand, the number of correct spikes is also considerably smaller. This is due to the fact that the spikes preceding a given spike in a sequence are also succeeding it because of the periodic presentation of the sequences (see, e.g., Fig. 3). Synapses between the corresponding neurons are therefore enhanced as well as depressed. For shorter sequences the last presentation of the sequence is closer and therefore the depression effect stronger, leading to lesser overall synapse strength (cf. Fig. 12). This creates the fewer retrieved spikes for shorter sequences in Fig. 11. To some extent this can be seen as an artifact because longer learning time or slightly larger learning increments A_+ could diminish this effect. On the other hand, this might have negative effects on the performance of the system in other parameter regions.

IV. ROBUSTNESS

Biological neural systems are subject to various external and internal noise sources. Starting from internal thermal noise within the system, this ranges over noisy or unreliable input and influences from other parts of the organism up to external electromagnetic fields. To test the effect of noise on the learning success of our model systems we focused on two types of noise. We implemented a Gaussian white noise in the membrane potential of the integrate-and-fire neurons and we implemented unreliable input.

The internal white noise was added to the membrane potential of each neuron independently. It is fully characterized by its mean 0 mV and its variance for which several values between 0.2 mV and 1.0 mV were tested.

To simulate unreliable input we implemented Poisson input neurons. These neurons produce rectangular spikes of width $t_{\text{spike}} = 3$ ms as before but the time of spiking is sto-

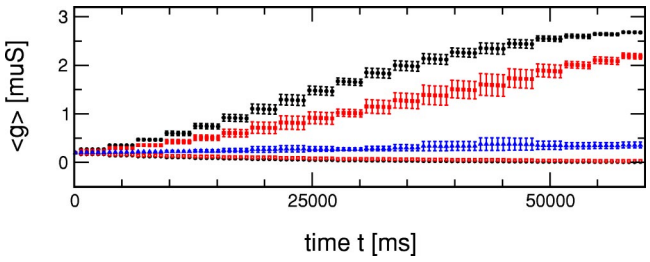

FIG. 12. Development of synaptic strength during training of a sequence of length 6 with speed $\Delta t = 10$ ms. The network of 50 neurons was trained with five sequences of length 6 in sequential order. Each sequence was presented for $80\Delta t$ at a time. The data shown are average synaptic strengths of synapses between the neurons of one of the trained sequences. The topmost points are the average strengths of all synapses between the neurons and their direct successors in the sequence, the middle are the corresponding strengths of synapses between neurons that are next nearest neighbors in the sequence under consideration, and the lower points correspond to strengths of synapses between neurons with distance 3 in the sequence. Note how the synaptic strength for these synapses is suppressed because a spike, being the third predecessor of a given spike, is also the third successor of this spike due to cyclic training. The lowest data points are the strengths between the neurons of the sequence as described above but *against* the order of activation in the trained sequence.

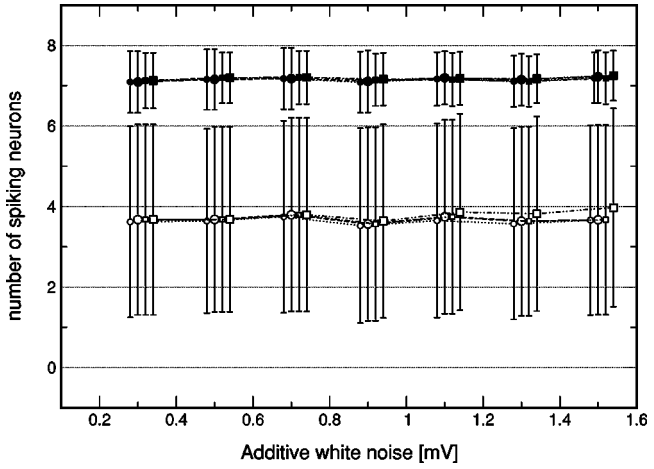

FIG. 13. Impact of Gaussian white noise in the membrane potential. The data points are the number of spiking neurons within tested sequences after $2400\Delta t$ training at $\Delta t = 10$ ms (full symbols) and the number of erroneously spiking neurons (open symbols). The small symbols were obtained when the noise was only present during learning and the large ones when noise was always present. The circles correspond to a cue of two inputs in testing and the squares to a cue of three inputs.

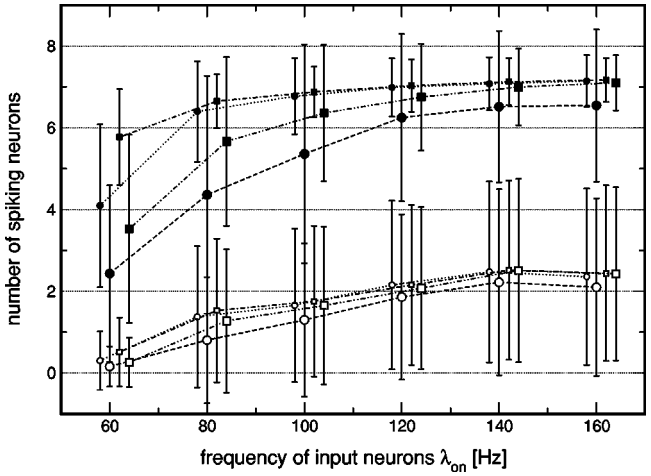

FIG. 14. Impact of noisy input on the learning performance. The input sequences were provided by stochastic Poisson neurons, as described in the text. The data points are the number of spiking neurons within tested sequences after $2400\Delta t$ training at $\Delta t = 10$ ms (full symbols) and the number of erroneously spiking neurons (open symbols). The small symbols were obtained when the stochasticity of the input was only present during learning and the large ones when input was always stochastic. The circles correspond to a cue of two inputs in testing and the squares to a cue of three inputs.

chastic. The spike times are determined by the Poisson distribution:

$$P(n_{\text{spike}}=k)=e^{-\lambda t}\frac{(\lambda t)^k}{k!}, \tag{20}$$

where n_{spike} is the number of spikes occurring in an interval of length t and parameter λ is the mean firing rate. For small t this can be approximated by $P(n_{\text{spike}}=1)=\lambda t$, $P(n_{\text{spike}}=0)=1-\lambda t$, and $P(n_{\text{spike}}=k)=0$ for $k>1$. This is the probability distribution we use to decide whether a neuron fires within a time step of the Runge-Kutta algorithm used. After firing, the neurons are refractory for $t_{\text{refract}}=10$ ms. The training protocol is that the mean firing rate of the first neurons is switched from 0 to some activity level λ_{on} for $2\Delta t$, the next neuron is switched on after Δt for also $2\Delta t$, and so on. Different reliability of the input can be adjusted by parameter λ_{on}.

Figures 13 and 14 show the impact of the two types of noise on the learning performance. Figure 13 shows the effect of additive white noise at the membrane potential in the learning stage and in both learning and recalling. As mentioned, the standard deviation of the noise was chosen between 0.3 mV and 1.5 mV. The system seems to be more or less unaffected by noise of this magnitude. As expected, the learning is even less sensitive to noise than the recalling due to the fact that the effect of the temporally uncorrelated noise on the synaptic strength is averaged out over time.

Figure 14 shows the learning success if the input neurons fire stochastically during learning only and during learning and recall, as described above. Parameter λ_{on} was varied from 60 Hz to 160 Hz. The stochastic firing of the input neurons seem to only affect the overall number of spikes, i.e., correct spikes as well as incorrect ones but not their ratio. This indicates that mainly, missing input spikes during the training and especially during testing are responsible for the decreased spikes in the response. It is to be expected that longer training can diminish these effects even more. Like in the case of noise in the membrane potential, the learning stage is not affected as much by the noisy input as the recall. Again the same argument applies; the effects of the stochasticity of the input spikes is averaged out over time during the multiple repetitions in the training phase.

V. DISCUSSION

It has been demonstrated that STDP allows the transformation of temporal information into spatial information, providing an efficient mechanism for storing temporal sequences which does not require a sophisticated network topology. It is, however, not obvious how to *quantify* the storage capacity of the system from the observed recall performance for different numbers of stored sequences. Taking the heuristic rule that storage is successful if there are on average one or fewer incorrect spikes in recall, the capacity of a system of 50 neurons is about 5–6 sequences (see Fig. 10). The capacity estimates for $n=50$ and $k=8$ are $r(8,50,\frac{1}{2})\approx 6.3$ and $\hat{r}(8,50,\frac{1}{2})\approx 2.6$. The storage capacity of the system therefore seems to be mainly limited by the statistical properties of the input, i.e., the overlap probabilities for randomly chosen input sequences. The biologically found STDP learning rule obviously does not imply severe restrictions on the ability to learn sequences but, on the contrary, seems to be very well suited for this task. There are indications that the learning mechanism is even more reliable with biologically more realistic conductance based model neurons

that have nontrivial intrinsic dynamics which to some extent prevents the speedup in recall, already discussed above.

The successful storage of arbitrary input sequences, however, crucially depends on the existence of the corresponding synapses, making the weak all-to-all connections in the investigated system a necessary requirement. For real biological systems, the global all-to-all connections are an approximation of the real connectivity and divergence and redundancy of the input. If the density of connections and the number of neurons each input excites is high enough, pairs of connected neurons being excited by successive inputs appear on a statistical basis. Preliminary results for the known connectivity in the olfactory system of locust support this idea. It will be discussed more thoroughly in forthcoming work [50].

The global inhibition is not so crucial in this study. It can be realized even more realistically by local interneurons activated by the average activity of the neighboring principal neurons. As the role of the inhibition in this system is just to control the activity of a highly excitable network and not to organize precise synchronous firing or any other sophisticated function, it does not really matter how well coordinated this inhibition is throughout the system. Especially, if the excitatory connections cease to be all-to-all in a more realistic setup the inhibitory circuit can easily be local as well. On the other hand the example of the locust, where a strong, periodic, global feed-forward inhibition onto the Mushroom Body is provided through synchronized Lateral Horn interneurons, shows that global inhibition is not necessarily unrealistic [51].

The realistic implementation of saturation of synaptic strength for additive learning rules is another important topic. For the system investigated here, we implemented a combination of two mechanisms. On the one hand the synaptic strength was directly bounded by use of the sigmoid filtering function applied to the bare synaptic strength subject to the additive learning rule, a technique commonly used by biologists. On the other hand the steady decay of synaptic strength and the continuous stimulation of the network by the inputs lead to a dynamical steady state, thereby bounding the synaptic strength dynamically.

Whereas the direct bound through a sigmoid filtering function might capture some aspects of the behavior of real synapses, the decay of synaptic strength necessary to achieve a realistic dynamical steady state is clearly too fast to be realistic. The system forgets much too fast if it is not continuously stimulated with appropriate input.

Alternative solutions to the saturation problem include competition based mechanisms suggested by recent findings of interactions of various kinds between neighboring synapses on a dendritic tree [52] and learning rules that depend on the synaptic strength itself, e.g., multiplicative learning rules.

The system is reasonably robust against noise. It is noteworthy that it is not very sensitive to internal high-frequency noise. In the range of noise applied in our trials, the recall barely depended on the level of noise (see Fig. 13). Whether this is an effect of the integrate-and-fire neuron model used here is beyond the scope of this work. The tolerance to biologically more relevant noise in the spike timing of the input is also rather impressive, taking into account that $\lambda_{on} = 60$ Hz corresponds to a total firing probability of only 36% for each of the input neurons within their activity window of 20 ms. Nevertheless, the system still was able to store at least parts of the presented sequences at this high noise level.

ACKNOWLEDGMENTS

We thank Walter Senn for numerous helpful remarks and suggestions. This work was partially supported by the U.S. Department of Energy, Office of Basic Energy Sciences, Division of Engineering and Geosciences, under Grant Nos. DE-FG03-90ER14138 and DE-FG03-96ER14592, by grants from the National Science Foundation, NSF PHY0097134 and NSF EIA0130708, by a grant from the Army Research Office, DAAD19-01-1-0026, by a grant from the Office of Naval Research, N00014-00-1-0181, and by a grant from the National Institutes of Health, NIH R01 NS40110-01A2.

APPENDIX: TAYLOR EXPANSION OF p_i^j

We first need to prove identity

$$\frac{d^n}{dx^n}\binom{r}{s}x^s(1-x)^{r-s}=\sum_{k=\max\{n+s-r,0\}}^{\min\{s,n\}}\binom{r}{s}\frac{s!}{(s-k)!}\frac{(r-s)!}{(r-s-(n-k))!}\binom{n}{k}(-1)^{n-k}x^{s-k}(1-x)^{r-s-(n-k)}. \tag{A1}$$

The proof is by induction. Let $n=0$. Then the equation reduces to

$$\binom{r}{s}x^s(1-x)^{r-s}=\binom{r}{s}\frac{s!}{s!}\frac{(r-s)!}{(r-s)!}\binom{0}{0}(-1)^0x^s(1-x)^{r-s}, \tag{A2}$$

which is clearly true. Assuming the validity of Eq. (A1) for n we can calculate

$$\frac{d^{n+1}}{dx^{n+1}}\binom{r}{s}x^s(1-x)^{r-s}=\frac{d}{dx}\left(\sum_{k=\max\{n+s-r,0\}}^{\min\{s,n\}}\binom{r}{s}\frac{s!}{(s-k)!}\frac{(r-s)!}{(r-s-(n-k))!}\binom{n}{k}(-1)^{n-k}x^{s-k}(1-x)^{r-s-(n-k)}\right) \tag{A3}$$

$$=\sum_{k=\max\{n+s-r,0\}}^{\min\{s,n\}}\binom{r}{s}\frac{s!}{(s-k-1)!}\frac{(r-s)!}{(r-s-(n-k))!}\binom{n}{k}(-1)^{n-k}x^{s-k-1}(1-x)^{r-s-(n-k)} \tag{A4}$$

$$+\sum_{k=\max\{n+s-r,0\}}^{\min\{s,n\}}\binom{r}{s}\frac{s!}{(s-k)!}\frac{(r-s)!}{(r-s-(n+1-k))!}\binom{n}{k}(-1)^{n+1-k}x^{s-k}(1-x)^{r-s-(n+1-k)}. \tag{A5}$$

Shifting the index in the first sum by one, using the well known identity $\binom{n}{k}+\binom{n}{k-1}=\binom{n+1}{k}$ and obvious identities such as $1=\binom{n+1}{0}$ one obtains Eq. (A1) for $n+1$, which completes the proof.

The Taylor expansion for p_j^i is then straightforward:

$$p_j^i=1-\sum_{s=0}^{i-1}\binom{r}{s}p_j^s(1-p_j)^{r-s} \tag{A6}$$

$$=-\sum_{n=1}^{\infty}\sum_{s=0}^{i-1}\left(\sum_{k=\max\{n+s-r,0\}}^{\min\{s,n\}}\binom{r}{s}\frac{s!}{(s-k)!}\frac{(r-s)!}{(r-s-(n-k))!}\binom{n}{k}(-1)^{n-k}p_j^{s-k}(1-p_j)^{r-s-(n-k)}\right)\Bigg|_{p_j=0}\frac{(p_j)^n}{n!}. \tag{A7}$$

For all $k<s$ the nth derivative contains a nonzero power of p_j and is thus $=0$ at $p_j=0$. Furthermore, if $s>n$ then all k are less then s and therefore, the whole sum over k is empty. We end up with

$$p_j^i=-\sum_{n=1}^{\infty}\sum_{s=0}^{\min\{i-1,n\}}\binom{r}{s}\frac{s!(r-s)!}{(r-n)!}\binom{n}{s}(-1)^{n-s}\frac{(p_j)^n}{n!} \tag{A8}$$

$$=-\sum_{n=1}^{\infty}\sum_{s=0}^{\min\{i-1,n\}}\binom{r}{n}\binom{n}{s}(-1)^{n-s}(p_j)^n. \tag{A9}$$

For any $n\leqslant i-1$ the inner sum is

$$\binom{r}{n}(p_j)^n\sum_{s=0}^{n}\binom{n}{s}(-1)^{n-s}1^s=\binom{r}{n}(p_j)^n(1-1)^n=0. \tag{A10}$$

Therefore, the leading term of the Taylor expansion of p_j^i is

$$p_j^i=\binom{r}{i}(p_j)^i+\mathcal{O}((p_j)^{i+1}). \tag{A11}$$

[1] R.H.R. Hahnloser, A.A. Kozhevnikov, and M.S. Fee, Nature (London) **419**, 65 (2002).

[2] A.S. Dave, A.C. Yu, and D. Margoliash, Science **282**, 2250 (1998).

[3] A.C. Yu and D. Margoliash, Science **273**, 1871 (1996).

[4] R. Van Rullen and S.J. Thorpe, Neural Comput. **13**, 1255 (2001).

[5] G. Laurent, K. MacLeod, and M. Wehr, Neurobiol. Learn Mem. **5**, 124 (1998).

[6] G. Laurent, Science **286**, 723 (1999).

[7] G. Laurent, M. Stopfer, R.W. Friedrich, M.I. Rabinovich, and H.D.I. Abarbanel, Annu. Rev. Neurosci. **24**, 263 (2001).

[8] J.A. Hertz, R.G. Palmer, and A.S. Krogh, *Introduction to The Theory of Neural Computation* (Addison-Wesley, Redwood City, CA, 1991).

[9] T.P. Trappenberg, *Fundamentals of Computational Neuroscience* (Oxford University Press, New York, 2002).

[10] P. Vetter, A. Roth, and M. Hausser, J. Neurophysiol. **85**, 926 (2001).

[11] M. Häusser, N. Spruston, and G.J. Stuart, Science **290**, 739 (2000).

[12] C. Koch, *Biophysics of Computation: Information Processing in Single Neurons* (Oxford University Press, New York, 1999).

[13] C. Koch, Biol. Cybern. **50**, 15 (1984).

[14] L.A. Jeffres, J. Comp. Physiol. Psychol. **41**, 35 (1948).

[15] H. Sompolinsky and I. Kanter, Phys. Rev. Lett. **57**, 2861 (1986).

[16] A. Herz, B. Sulzer, R. Kühn, and J.L. van Hemmen, Europhys. Lett. **7**, 663 (1988).

[17] A. Herz, B. Sulzer, R. Kühn, and J.L. van Hemmen, Biol. Cybern. **60**, 457 (1989).

[18] W. Gerstner, R.R. Ritz, and J.L. van Hemmen, Biol. Cybern. **69**, 503 (1993).

[19] J. Hertz and A. Prügel-Bennett, Network Comput. Neural Syst. **7**, 357 (1996).

[20] C. Leibold, R. Kempter, and J.L. van Hemmen, Phys. Rev. E **65**, 051915 (2002).

[21] J. Rinzel, D. Terman, X. Wang, and B. Ermentrout, Science **279**, 1351 (1998).

[22] D. Colomb, X.J. Wang, and J. Rinzel, J. Neurophysiol. **75**, 750 (1996).
[23] J.E. Lisman and N.A. Otmakhova, Hippocampus **11**, 551 (2001).
[24] J.E. Lisman, Neuron **22**, 233 (1999).
[25] S.P. Tonkin and R.B. Pinter, Network Comput. Neural Syst. **7**, 385 (1996).
[26] R.P.N. Rao and T.J. Sejnowski, in *Advances in Neural Information Processing Systems*, edited by S.A. Solla, T.K. Leen, and K.-R. Muller (MIT Press, Cambridge, MA, 2000), Vol. 12, pp. 164–170.
[27] L.F. Abbott and K.I. Blum, Cereb. Cortex **6**, 406 (1996).
[28] M.R. Mehta, C.A. Barnes, and B.L. McNaughton, Proc. Natl. Acad. Sci. U.S.A. **94**, 8918 (1997).
[29] W. Gerstner and L.F. Abbott, J. Comput. Neurosci. **4**, 79 (1997).
[30] O. Jensen and J.E. Lisman, Neurobiol. Learn Mem. **3**, 279 (1996).
[31] M. Rabinovich, A. Volkovskii, P. Lecanda, R. Huerta, H.D.I. Abarbanel, and G. Laurent, Phys. Rev. Lett. **87**, 068102 (2001).
[32] R.C. Malenka and R.A. Nicoll, Science **285**, 1870 (1999).
[33] D.J. Linden, Neuron **22**, 661 (1999).
[34] G.-q. Bi and M.-m. Poo, Annu. Rev. Neurosci. **24**, 139 (2001).
[35] S.-N. Yang, Y.-G. Tang, and R.S. Zucker, J. Neurophysiol. **81**, 781 (1999).
[36] H. Markram, J. Lübke, M. Frotscher, and B. Sakmann, Science **275**, 213 (1997).
[37] G.-q. Bi and M.-m. Poo, J. Neurosci. **18**, 10 464 (1998).
[38] J. Lisman, Proc. Natl. Acad. Sci. U.S.A. **86**, 9574 (1989).
[39] W.R. Holmes and W.B. Levy, J. Neurophysiol. **63**, 1148 (1990).
[40] A.M. Zador, C. Koch, and T.H. Brown, Proc. Natl. Acad. Sci. U.S.A. **87**, 6718 (1990).
[41] J.I. Gold and M.F. Bear, Proc. Natl. Acad. Sci. U.S.A. **91**, 3941 (1994).
[42] A. Schiegg, W. Gerstner, and J.L. van Hemmen, J. Neurophysiol. **74**, 1046 (1995).
[43] H.Z. Shouval, M.F. Bear, and L.N. Cooper, Proc. Natl. Acad. Sci. U.S.A. **99**, 10831 (2002).
[44] H.D.I. Abarbanel, R. Huerta, and M.I. Rabinovich, Proc. Natl. Acad. Sci. U.S.A. **99**, 10132 (2002).
[45] W. Rall, J. Neurophysiol. **30**, 1138 (1967).
[46] W. Rall, in *Methods in Neuronal Modeling: From Synapses to networks*, edited by C. Koch and I. Segev (MIT Press, Cambridge, 1989), pp. 9–62.
[47] A. Destexhe, Z. F. Mainen, and T. J. Sejnowski, in *Methods in Neuronal Modeling*, 2nd ed., edited by C. Koch and I. Segev (MIT Press, Cambridge, MA, 1998), pp. 1–26.
[48] J. C. Butcher, *The Numerical Analysis of Ordinary Differential Equations* (Wiley, Chichester, 1987).
[49] T. Nowotny, M. I. Rabinovich, and H. D. I. Abarbanel, in *SfN Annual Meeting 2002, Abstracts* (Society for Neuroscience, Oralando, FL, 2002).
[50] T. Nowotny, M. I. Rabinovich, R. Huerta, and H. D. I. Abarbanel (unpublished).
[51] J. Perez-Orive, O. Mazor, G.C. Turner, S. Cassenaer, R.I. Wilson, and G. Laurant, Science **297**, 359 (2002).
[52] N. Arnth-Jensen, D. Jabaudon, and M. Scanziani, Nat. Neurosci. **5**, 325 (2002).